Biomimetic 3D-printed scaffolds for spinal cord injury repair

Jacob Koffler[1,6,*], **Wei Zhu**[2,6], **Xin Qu**[2], **Oleksandr Platoshyn**[3], **Jennifer N. Dulin**[1], **John Brock**[1], **Lori Graham**[1], **Paul Lu**[1], **Jeff Sakamoto**[4], **Martin Marsala**[3], **Shaochen Chen**[2,*], and **Mark H. Tuszynski**[1,5,*]

[1]Department of Neuroscience, University of California San Diego, La Jolla, CA, USA.

[2]Department of NanoEngineering, University of California San Diego, La Jolla, CA, USA.

[3]Department of Anesthesiology, University of California San Diego, La Jolla, CA, USA.

[4]Mechanical Engineering Department, University of Michigan, Ann Arbor, MI, USA.

[5]Veterans Affairs Medical Center, San Diego, CA, USA.

[6]These authors contributed equally: Jacob Koffler and Wei Zhu.

Abstract

Current methods for bioprinting functional tissue lack appropriate biofabrication techniques to build complex 3D microarchitectures essential for guiding cell growth and promoting tissue maturation[1]. 3D printing of central nervous system (CNS) structures has not been accomplished, possibly owing to the complexity of CNS architecture. Here, we report the use of a microscale continuous projection printing method (μCPP) to create a complex CNS structure for regenerative medicine applications in the spinal cord. μCPP can print 3D biomimetic hydrogel scaffolds tailored to the dimensions of the rodent spinal cord in 1.6 s and is scalable to human spinal cord sizes and lesion geometries. We tested the ability of μCPP 3D-printed scaffolds loaded with neural progenitor cells (NPCs) to support axon regeneration and form new 'neural relays' across sites of complete spinal cord injury in vivo in rodents[1,2]. We find that injured host axons regenerate into 3D biomimetic scaffolds and synapse onto NPCs implanted into the device and that implanted NPCs in turn extend axons out of the scaffold and into the host spinal cord below the injury to

restore synaptic transmission and significantly improve functional outcomes. Thus, 3D biomimetic scaffolds offer a means of enhancing CNS regeneration through precision medicine.

More than 500,000 people in the United States suffer from spinal cord injury (SCI), with resulting substantial psychological and economic costs[3]. 3D printing technology allows the fabrication of personalized scaffolds that 'fit' the precise anatomy of an individual's injury to stimulate, guide and align axon regeneration. Common inkjet or extrusion bioprinting creates simple structures such as cartilage or blood vessels[4], but µCPP can create complex 3D architectures using a variety of biomaterials and cells[5] (Fig. 1a) in one continuous print (Fig. 1b). Inkjet or extrusion printing can compromise the mechanical integrity through artificial interfaces between drops or lines; µCPP layerless printed structures do not exhibit planar artifacts (interfaces). Only 1.6 s is required to print a 2-mm scaffold (Supplementary Video 1), a rate ~1,000× faster than traditional nozzle printers[5]. Using focused light for polymerization generates a printing resolution of 1 µm.

We designed a rat spinal cord scaffold to support regeneration after injury (Fig. 1a). Microchannels of 200 µm in diameter provide alignment with host axonal tracts above and below the injury (Fig. 1d,e). The inner 'gray matter' area of the spinal cord is normally free of axons projecting below the injury site; thus, we made this area solid to enhance the structural integrity (Fig. 1d). Scaffolds exhibited an elastic modulus of 260–300 kPa (Fig. 1k), similar to normal spinal cord (200–600 kPa)[6–8].

For proof of concept, we printed scaffolds that conform to the precise shape and dimensions of several different and complex human spinal cord lesion cavities, including contusion lesions (Fig. 1f–j and Supplementary Fig. 1b) and a knife cut (Supplementary Fig. 1b).

We then implanted scaffolds into rats with T3 complete spinal cord transection[9]. Eleven Fischer rats underwent placement of 2-mm-long 3D biomimetic scaffolds into the lesion; eleven received 3D biomimetic scaffolds fabricated from polyethylene glycol-gelatin methacrylate (PEG-GelMA) loaded with NPCs; eight controls underwent lesions only; eight controls received rat NPCs without scaffolds; and seven animals received agarose scaffolds containing 200-µm channels (previous generation of scaffolds[9–14]) for comparison to 3D PEG-GelMA printed scaffolds. Four weeks later, the channels and solid core of 3D biomimetic scaffolds retained their pre-implantation structure without breakage or deformation (Fig. 2a). 3D biomimetic scaffolds comprised of other materials, including hyaluronic acid, rapidly degraded and collapsed after 4 weeks (Supplementary Fig. 2). Maintenance of scaffold structure over at least four weeks is considered essential to retain physical support across a lesion site and to align regenerating axons across the lesion. PEG-GelMa scaffolds were also biocompatible, exhibiting a significant attenuation of reactive cell layers and granularized tissue that formed around templated agarose scaffolds (Fig. 2b and Supplementary Fig. 2). The thickness of host reactive cell layers around 3D biomimetic scaffolds was also attenuated by 35% compared to agarose scaffolds ($P < 0.05$; Fig. 2b, right). Scaffold implantation did not exacerbate the spinal cord inflammatory response, as shown by IBA1 labeling for microglia and macrophages (Supplementary Fig. 3).

Importantly, reactive astrocyte responses were modified by 3D biomimetic scaffolds: in control lesions and recipients of agarose scaffolds, a layer of reactive astrocytes 'walled off' the lesion (Fig. 2c, left). In contrast, astrocytic processes were rearranged by 3D-printed scaffolds and no longer formed a 'wall' at the host/scaffold interface; instead, astrocyte processes were strikingly realigned longitudinally with open channels of the scaffolds, oriented along the axis of axons penetrating into scaffold channels (Fig. 2c, right, and Supplementary Fig. 4). Moreover, quantification of total glial fibrillary acidic protein (GFAP) immunoreactivity at the host/lesion/graft interface revealed a significant reduction among animals implanted with 3D biomimetic printed scaffolds compared to other lesioned animals ($P < 0.05$; Fig. 2c, right).

Toluidine blue and RECA-1 immunolabeling showed that empty scaffolds were readily and extensively vascularized (Fig. 2d).

Injured host axons labeled for neurofilament-200 (NF200) regenerated into empty 3D biomimetic scaffolds, readily passing across host/scaffold interfaces. Axons penetrating the scaffold grew in linear orientations along the rostral-to-caudal axis of the spinal cord, guided by scaffold walls (Fig. 2e, right); this was in contrast to frequent axonal misalignment and deflection at the interfaces of agarose scaffolds with the host[10,11] (Fig. 2e, left). The mean number of neurofilament-labeled regenerating axons per channel in 3D biomimetic scaffolds was 97 ± 8, quantified 1 mm from the rostral host/scaffold interface. Host serotonergic axons also regenerated into the scaffold (Fig. 2f, left), and a mean of 11 ± 5 serotonergic axons reached the caudal end of the scaffold (Fig. 2f, right). Host Schwann cells from the peripheral nervous system[11] migrated into the scaffolds and ensheathed or remyelinated many regenerating host axons (Fig. 2g–i).

Neural stem cells (NSCs) and NPCs have emerged as a means of enhancing regeneration of lesioned host axons into SCIs[1,2,15,16]. Activity from lesioned host axons above the injury can be transmitted across the lesion to host neurons below the injury via relays formed by implanted NSCs, supporting functional improvement[1,2,15,16]. Previously we grafted NPCs 2 weeks after injury because dissociated cell grafts survived poorly in acute lesion sites[1,2,15,16], due to toxic blood products and inflammation[17–21]; these responses are reduced after subacute delays[18,19,22,23]. Scaffolds might protect grafted cells, offering the possibility of intervening acutely after injury, when patients undergo spinal decompression and stabilization[24,25]. To test this hypothesis, we grafted NSCs within scaffolds to acute SCI lesion sites, loading GFP-expressing rat NPCs ($n = 11$ animals; see Methods)[1,2,16]. An additional set of animals received grafts of NPCs into the lesion site without scaffolds ($n = 8$ animals).

One month later, NPCs survived in every grafted animal and completely filled the scaffold channels (Fig. 3a and Supplementary Fig. 5a). NSCs were also present at interfaces between the scaffolds and host spinal cord, without distorting the scaffold or host spinal cord architecture (Supplementary Fig. 5a). A total of $47 \pm 2\%$ of grafted NPCs expressed the early neuronal marker Hu[1] (Supplementary Fig. 5b,f), $20 \pm 3\%$ expressed the mature neuronal marker NeuN (Supplementary Fig. 5c,f), $21 \pm 3\%$ expressed the astrocyte marker GFAP (Supplementary Fig. 5d–f) and $11 \pm 2\%$ expressed the oligodendrocyte marker Olig2

(Supplementary Fig. 5e,f). The stem state marker nestin was not detected, as expected following graft differentiation. A total of 2.8% of implanted cells labeled for the dividing cell marker Ki67. Among animals that received NPC grafts without scaffolds, some cells survived but invariably failed to fill the lesion site, leaving very large gaps (Supplementary Fig. 5a). Thus, implantation of NPCs into early lesion sites is feasible with scaffolds, but fails without scaffolds, consistent with previous reports using dissociated or solid cell grafts[18–22]. Scaffolds appear to provide a protected environment, probably free of acute inflammatory mediators and reactive oxygen species[26].

Very large numbers of neurofilament-labeled axons regenerated in scaffolds loaded with NPCs (Fig. 3b). Regenerating host axons aligned into parallel linear arrays, adopting a pattern mimicking the linear axonal alignment of the intact spinal cord (Fig. 3b). Host serotonergic axons, which modulate spinal motor systems, also regenerated into 3D biomimetic scaffolds loaded with NPCs (Fig. 3d) and extended linearly from the rostral to caudal aspects of scaffolds in significantly greater numbers when scaffolds were loaded with NPCs: a mean of 85 ± 21 serotonergic axons per channel reached the end of the lesion and extended into the distal host spinal cord in animals with guidance scaffolds and NPCs, whereas 8-fold fewer axons (a mean of 11 ± 5 axons) reached the end of the lesion in empty scaffolds (Fig. 3g). Among animals implanted with NPCs without a scaffold, serotonergic axons grew in random rather than linear orientations (Supplementary Fig. 5g) and did not reach the caudal side of the lesion (ANOVA $P < 0.0322$ comparing all groups; post hoc Tukey's; Fig. 3g). Thus, 3D biomimetic scaffolds plus NPC grafts significantly enhance host axonal regeneration into, and occasionally beyond, the lesion (Fig. 3e). Serotonergic axons located in the host spinal cord caudal to the lesion were not graft-derived, since NPCs in the scaffold did not immunolabel for 5-hydroxytryptamine (5HT; serotonin), and serotonergic axons did not co-label for GFP (Supplementary Fig. 5h). At 2 mm beyond the scaffold, serotonergic axons were detected in white and gray matter of the host spinal cord (Supplementary Fig. 5i) and could be detected up to 3.5 mm beyond the lesion site but not beyond, indicating that these were regenerating (not spared) axons.

NPC-derived axons were identifiable with GFP labeling and were abundant within channels and grew linearly (Fig. 3 c). In contrast, NPC grafts placed into lesion sites without scaffolds extended axons in random directions (Supplementary Fig. 6). Axons from implanted NPCs extended out from scaffolds in large numbers into the host spinal cord in both caudal and rostral directions (Supplementary Fig. 5j).

Ultrastructural analysis of axons in NPC-filled channels at 4 weeks post-implantation demonstrated a range of axon calibers and myelination states, from small, unmyelinated axons (<1 μm diameter) to large axons (1–3 μm, Fig. 3h), in some cases myelinated by oligodendrocytes (Fig. 3i and Supplementary Fig. 7a). Asymmetric synapses within scaffolds formed and contained rounded synaptic vesicles, typical of excitatory synapses (Fig. 3j)[27–29]. Host serotonergic axons regenerating into channels were closely associated with dendrites of NPC-derived neurons, identified by co-labeling for MAP2 and GFP (Fig. 3f).

Toluidine blue and ultrastructural analysis demonstrated vascularization within NPC-loaded scaffolds at 4 weeks post-implantation (Supplementary Fig. 7b). Astrocytic end-feet were observed in contact with blood vessels, together with pericytes and tight junctions (Supplementary Fig. 7c,d). Thus, blood vessels were fenestrated and the blood-brain barrier was restored[30,31].

We proceeded to long-term functional studies. A total of 22 rats underwent T3 complete transections and received acute implants of either 3D biomimetic scaffolds loaded with rat spinal cord NPCs ($n = 11$) or empty scaffolds ($n = 11$). Another group ($n = 11$) underwent grafting of NPCs without scaffolds to the acute lesion site[1,2]. We did not include lesion-only controls, to keep animal numbers manageable, and because empty scaffolds supported only limited host axon growth into scaffolds.

Anatomical analysis 6 months later showed that scaffolds retained their 3D architecture (Fig. 4a). Scaffold wall thickness was reduced by 49% compared with pre-implantation size (Supplementary Fig. 8b), reflecting slow degradation. Notably, NPCs survived and filled scaffold channels. In contrast, grafts to lesions without scaffolds incompletely survived and filled the lesion (Supplementary Fig. 8a), leaving large cavities. Thus, implantation of 3D-printed scaffolds into acute SCI enables consistent stem cell survival and filling of the site, despite an acute environment that is inflammatory and cytotoxic[26]. Among animals implanted with empty scaffolds, host neurofilament-labeled axons regenerated into scaffolds (Supplementary Fig. 8c) in relatively modest numbers (118 ± 8), similar to numbers observed 4 weeks after implantation (97 ± 8 axons). In no case did host axons regenerate beyond the scaffold and into the distal host spinal cord (data not shown) in animals implanted with empty scaffolds. Among animals implanted with 3D biomimetic scaffolds loaded with NPCs, grafted cells survived through the 6-month period and completely filled the channels (Fig. 4a). Nestin labeling was not detected, indicating maturation of implanted NPCs, and Ki67 labeling was also not detected, indicating completion of cell division. As observed in 4-week scaffolds, 5HT-immunoreactive axons entered the scaffold (Supplementary Fig. 8d). At total of 87 ± 5 serotonergic axons reached the caudal end of channels loaded with NPCs and continued to regenerate into the caudal spinal cord, similar to the numbers of axons observed 4 weeks after implantation (Fig. 3g and Supplementary Fig. 8d); this observation suggests that serotonergic axon regeneration into scaffolds is complete by 4 weeks. Host corticospinal motor axons, anterogradely labeled by injections of AAV2-RFP vectors into the motor cortex, also regenerated into NPC-loaded scaffolds (Fig. 4b) and extended to scaffold midpoints, a distance of 1 mm (Supplementary Fig. 8e). Corticospinal axons formed putative bouton-like structures on NeuN-labeled neurons within the scaffold channels (Fig. 4c), consistent with previous reports that host corticospinal axons regenerating into NPC grafts form VGlut1-labeled excitatory appositions within grafted neurons[1]. Moreover, graft-derived GFP-labeled axons projected out from the scaffolds and into the host spinal cord caudal to the injury (Fig. 4d), forming close appositions with host neurons caudal to the lesion site that co-localized with the excitatory synaptic marker VGlut2 (Fig. 4e). The amount of graft-derived axonal outgrowth from scaffolds into the distal host spinal cord (Fig. 4d) greatly exceeded the number of host serotonergic axons regenerating beyond the scaffold (Supplementary Fig. 8d); this observation suggests that restored neural relays across the lesion site, if present, would most likely be mediated by

relays formed from host axons regenerating into the scaffold, synapsing onto grafted NPCs, and NPC-derived axons extending into the distal host spinal cord. Among animals that received acute NPC grafts without scaffolds, host axons labeled for neurofilament and serotonin also penetrated the partial graft fills of the lesion site (Supplementary Fig. 8f,g), but axons grew in random orientations rather than exhibiting the linear growth patterns observed in grafts within scaffolds (Supplementary Fig. 8f,g).

To determine whether 3D biomimetic scaffolds support motor functional recovery, animals were assessed using the Basso, Beattie and Bresnahan (BBB) locomotor scale[32] over a 5-month period. Animals that received scaffolds loaded with NPCs exhibited significant functional recovery compared to animals with empty scaffolds. The performance of animals with NPC grafts lacking scaffolds did not differ from that of animals implanted with empty scaffolds, indicating that the mere presence of stem cells is insufficient to support functional recovery when grafts fail to fill the lesion cavity and exhibit continuity from the rostral to the caudal end of the lesion (Fig. 4f). Functional scores reached a mean value of 6.6 ± 0.5 points ($\pm$ s.e.m.) on the BBB scale in animals that received NPCs in scaffolds, indicating movement about each joint of the hindlimb, in contrast to a mean score of 0.3 ± 0.2 points in empty scaffolds and 1.6 ± 0.8 in NPC graft controls, reflecting inconsistent movements around only one joint (*$P < 0.0001$, repeated-measures ANOVA; t-test for individual time points and post hoc Tukey's; Fig. 4f).

We further investigated the formation of neural relays via electrophysiological transmission across the complete transection site, by measuring myogenic motor evoked potentials (MEPs) from the hindlimbs in response to electrical stimulation of the brain (Fig. 4g,h)[33,34]. At 5 months post-injury, rats implanted with 3D biomimetic poly(ethylene glycol) diacrylate (PEGDA)-GelMa scaffolds loaded with NPCs exhibited recovery of motor evoked responses (mean MEP amplitude 270 ± 5 µV; mean latency 11.3 ± 0.7 ms), whereas animals implanted with empty scaffolds exhibited responses in the range of baseline noise (mean MEP amplitude 25.1 ± 5.7 µV, $P < 0.0001$, Student's two-tailed t-test; mean latency 15.3 ± 0.8 ms; $P < 0.0001$, Student's two-tailed t-test; Fig. 4g–i and Supplementary Fig. 9). Re-transection of the spinal cord at the C8 level (rostral to the implant site) resulted in loss of all evoked potentials in the hindlimbs (Fig. 4h), confirming the formation of new electrophysiological relays across the lesion.

This study demonstrates the feasibility of using rapid 3D printing to create biomimetic central nervous system structures. These scaffolds can be readily individualized and scaled to any patient-specific lesion shape and length. While we and others have noted the importance of guiding axons through a lesion site[10,13,35–37], here we demonstrate host axon regeneration entirely beyond a severe, complete spinal cord transection site supported by a bioengineered scaffold. Moreover, the scaffold supports engraftment of NPCs acutely after injury, when most spinal-cord-injured patients undergo surgical decompression; thus, 3D biomimetic PEGDA-GelMa scaffolds provide a potential means for intervening early with neural stem cell grafts after injury. The growth of regenerating host and stem cell-derived axons is strikingly linear as they traverse scaffolds.

While previous studies have introduced bioengineered scaffolds into sites of SCI[10–13,35–37], most reports fail to address host inflammatory responses to scaffolds. Notably, our PEGDA-GelMa scaffolds re-engineer the astrocyte response at the injury site, aligning host astrocytes with the growth axis of host axonal fascicles[38], rather than blocking axonal growth[39]. This may support the extensive host axonal regeneration into and, in the case of serotonergic host axons, out from the lesion site into the distal host spinal cord.

Methods

Scaffold materials

PEGDA (Mn = 700 Da) was purchased from Sigma-Aldrich.

GelMa was synthesized as described in previous reports[5]. The photoinitiator lithium phenyl-2,4,6-trimethylbenzoylphosphinate (LAP) was synthesized as previously reported[40]. The matrix material used for printing the scaffolds was made by mixing 7.5% (w/v) GelMa, 25% (v/v) PEGDA and 0.225% (w/v) LAP in Dulbecco's phosphate-buffered saline solution.

Scaffold 3D printing

The 3D bioprinter (μCPP) consists of the following six components as shown in Fig. 1b: an ultraviolet light-emitting diode light source (365 nm) for photopolymerization; a DMD chip (Texas Instruments) consisting of $1{,}920 \times 1{,}080$ micromirrors for optical pattern generation; projection optics for imaging the optical pattern on the DMD chip to the fabrication plane on the stage; an automatic stage holding the monomer solution for fabrication; a digital camera for real-time monitoring and imaging of the fabrication process; and a computer coordinating the ultraviolet light source, the DMD chip, the stage and the camera for the 3D-printing process.

Rat spinal cord scaffold printing

Digital images of gray and white matter were generated by processing the cross-section image of the T3 spinal rat spinal cord, which were later imported into the DMD chip to control the micromirrors during the printing process. Channels (200 μm in diameter) were incorporated into the white matter to provide linear guidance for the axonal regeneration. The gray matter was designed as a solid block of GelMa, 25% (v/v) PEGDA and 0.225% (w/v) LAP to enhance the mechanical strength of the printed scaffold. The monomer solution of the matrix material was loaded into a reservoir with a 2 mm polydimethylsiloxane spacer to control the z-axis height of the printed scaffolds. A continuous printing process was initiated using in-house-developed software for controlling the 3D printer. The scaffold was printed in two steps, 0.8 s long each, one for the white matter image and the next for the gray matter image (Supplementary Video 1). The printed scaffold was then removed from the reservoir and rinsed three times with sterile Dulbecco's phosphate-buffered saline and antibiotics (1% Pen Strep). We also tested 3D biomimetic scaffolds comprised of hyaluronic acid; however, those rapidly degraded and their structure collapsed after four weeks in vivo (Supplementary Fig. 2). Maintenance of scaffold structure over at least four weeks is considered essential to retain physical support across a lesion site

and to enable, organize and align the growth of regenerating axons. Accordingly, PEG-GelMa scaffolds emerged as our lead scaffold fabrication material for additional in vivo studies.

Human spinal cord scaffold printing

VA San Diego Institutional Review Board approved this retrospective study. Cervical magnetic resonance imaging scans from anonymous ASIA A patients were obtained from a database and used to model a typical chronic SCI. T1- and T2-weighted images were obtained. The lesion was traced and a 3D spinal cord computer-aided design model was used to match the human injury dimensions. The 3D model was then sliced into a series of digital masks along the longitudinal direction of the spinal cord, which were imported into the DMD chip sequentially. By dynamically changing the digital mask with the movement of the stage, the patient-specific spinal cord scaffold was using the methods described above.

Fabrication of templated agarose scaffolds

Agarose scaffolds were fabricated as previously described[10]. Multi-component fiber bundle templates were fabricated from 200-μm-diameter polystyrene fibers (Paradigm Optics) arranged in a hexagonal close-packed array separated by a continuous matrix of poly(methyl methacrylate), as previously described. They were arranged with 66-μm interval spacing in a honeycomb array to generate final scaffolds with wall sizes of 66 μm and channel diameters of 200 μm. Bundles were simultaneously extruded and fused such that polystyrene fibers were oriented parallel to the longitudinal axis of the bundles. The multi-component fiber bundle templates were trimmed to a length of 2 mm and a cross-sectional width and depth of 1.5 mm. Polystyrene end caps 1.5 mm in length were bonded to fiber bundle terminals using cyclohexane to anchor polystyrene fibers and form an external, rigid multi-component fiber bundle template. Six such multi-component fiber bundle units were then aligned in-series with two polystyrene side caps agglutinating into a linear template array. The poly(methyl methacrylate) matrix was then selectively removed by immersion in 99.7% propylene carbonate (Sigma-Aldrich) three times, followed by a 95% ethanol rinse and a distilled water rinse. Ultrapure agarose (30 mg ml^{-1}, Sigma-Aldrich) was dissolved in distilled water at 100 °C and then cooled to 65 °C. Multi-component fiber bundle templates were submerged into the agarose solution and centrifuged (300 r.p.m. for 30 s) to permeate agarose through the packed polystyrene fiber array. The agarose cast was then allowed to gel at room temperature, trimmed and immersed in 99% tetrahydrofuran (Sigma-Aldrich) at room temperature for 24 h. This was repeated twice to remove the polystyrene mold, resulting in individual free-floating agarose scaffolds. The scaffolds were collected and washed sequentially in acetone, 95% ethanol and three cycles of sterile water. They were stored in sterile water at room temperature until use.

Preparation of E14 NPCs

The cells were prepared as described previously[2]. Briefly, spinal cords from GFP-expressing E14 F344 embryos were dissected and the meninges were removed. The tissue was trypsinized for 15 min followed by centrifugation at 2,500 r.p.m. at room temperature. The tissue was resuspended in NeuroBasal medium (Gibco) containing 2% B27 (Gibco), and the spinal cord tissue was gently triturated using progressively smaller fire-polished Pasteur

pipettes. The cells were then centrifuged at 2,500 r.p.m. for 2 min, resuspended in NeuroBasal medium containing B27 and filtered using a 40-μm cell filter strainer.

Surgical procedures

National Institutes of Health and VA San Diego Institutional guidelines for laboratory animal care and safety were strictly followed. Scaffold implantation into a complete transection at the T3 spinal cord level was performed as previously described[9,10]. Briefly, animals were deeply anesthetized, and a T3 laminectomy was performed followed by a transection of the spinal cord using a combination of microscissors and microaspiration. A block of 1.8 mm was removed and a 2-mm-long scaffold was implanted; thus, the scaffold was retained securely between the transected segments of the spinal cord. The experimental groups for the four-week survival studies were: empty agarose scaffolds ($n = 7$); empty 3D-printed scaffolds ($n = 11$); 3D-printed scaffolds loaded with E14 NPCs ($n = 11$); rat E14-spinal cord-derived multipotent NPCs graft ($n = 8$); SCI, lesion only ($n = 8$). The experimental groups for the long-term survival studies were: empty 3D-printed scaffolds *(n = 11)*; rat E14-spinal cord-derived multipotent NPC graft (no scaffold) ($n = 11$); 3D-printed scaffolds loaded with E14 NPCs ($n = 11$).

Rat E14 NPCs were suspended in fibrin matrix containing a four-component growth factor cocktail: BDNF 50 ng μl^{-1} (Peprotech) to support NPC survival, VEGF 10 ng μl^{-1} (Peprotech) and bFGF 10 ng μl^{-1} (Peprotech) to promote angiogenesis, and MDL28170 50 μM (Sigma), a calpain inhibitor for neuroprotection[41]. Following the implant, the dorsal muscles and skin were sutured and antibiotics and analgesics were administered. A total of 3 $\times 10^6$ cells were directly loaded into scaffolds in a volume of 6 μl in 11 additional animals that underwent T3 complete transection, and animals were assessed later for scaffold integrity, cell survival and host axon regeneration and remyelination.

Functional studies

The BBB open-field 21-point locomotion rating scale was assessed weekly until it was stable by 2 independent observers blinded to group identity, over a 5-month period post-implantation[32]. Traditional BBB assessment enables scoring of a specific type of joint movement even if it occurs only once during a four-minute observation period. However, animals with complete spinal cord transection exhibit substantial spasticity, and reflex responses or twitches can occasionally occur that would be scored as positive responses under traditional criteria. To avoid the risk of scoring spastic responses or spontaneous twitches, we used a more conservative system and scored a response only if it occurred three times during the four-minute observation period.

Following the behavior stabilization observed by BBB, we measured MEPs in the hindlimbs during the following month (6 months post implant) as previously described[34]. Briefly, animals were anesthetized with propofol (100 mg kg^{-1}, PropoFlo Abbot) and transcranial electrical stimuli were applied using a pulse duration of 1 ms at 9 mV, using a DS3 constant current isolated stimulator (Digitimer). Stimuli were administered using two percutaneously placed 30G stainless-steel stimulation electrodes (Grass Technologies, Astro-Med, Inc.). MEPs were recorded by ring electrodes placed on both hindlimbs until the 3–5 stable and

repeatable recorded potentials were obtained. MEPs were recorded at week 26 post implant. For re-transection studies, animals were anesthetized, and the same protocol as stated above was followed. Once a MEP signal was recorded, the cervical region of the spinal cord was exposed, and a complete transection was made at the C8 level (above the implant site). We then followed the same recording protocol again to stimulate and record from both hindlimbs.

CST tracing

To label corticospinal axons in the spinal cord, adeno-associated virus vectors, serotype 2 (AAV2), expressing the reporter gene RFP, were injected into bilateral motor cortices three weeks before perfusion[42]. Using pulled-glass micropipettes (40 μm internal diameter) and a PicoSpritzer II (General Valve), 10 μl of AAV2-RFP was injected into 8 sites per hemisphere spanning the hindlimb rostrocaudal extent of the rat sensorimotor cortex, at a depth of 1.5 mm, as previously described[42]. The micropipette tip remained in place for 30 s before withdrawal.

Immunohistochemistry

Immunolabeling was performed as described previously[10]. Spinal cords were sectioned on a cryostat set at 20-μm intervals and processed for: GFP labeling, to assess grafted cell survival and differentiation and axon extension (GFP rabbit polyclonal, Invitrogen at 1:500); neural cell markers, including Hu for young neurons (human polyclonal at 1:500), NeuN for mature neuronal nuclei (mouse monoclonal, abcam at 1:500), MAP-2 for mature neurons (mouse monoclonal, BD Biosciences at 1:500), NF200 to label axons (mouse monoclonal, Millipore at 1:500), serotonin for mature neurons and axons (5HT, goat polyclonal, ImmunoStar, at 1:500), GFAP for astrocytes (chicken polyclonal, Millipore at 1: 500), Olig2 for oligodendrocytes (Olig2, mouse monoclonal, IBL at 1:200); S100 to label Schwann cells (rabbit polyclonal, Dako, at 1:500); Ki67 to label proliferating cells (rabbit polyclonal, Genetex at 1:500); nestin (mouse monoclonal, Genetex, at 1:500); IBA1 (rabbit polyclonal, Wako, at 1:500); VGlut2 (guinea pig polyclonal, at 1:500, Millipore). Sections were incubated overnight at room temperature for primary antibodies, followed by incubation in Alexa 488-, 594- or 647-conjugated goat or donkey secondary antibodies (1:250, Invitrogen) for 3 h at room temperature. The thickness of the reactive cell layer was measured in Nissl-stained sections under X200 total magnification. Eight sections per animal were quantified, with results expressed as mean ± s.e.m. GFAP immunoreactivity was quantified as the mean gray value per pixel^2 measured at the host spinal cord/ scaffold interface, on GFAP-immunolabeled sections. Eight sections per animal were quantified, with results expressed as mean ± s.e.m. 5HT axons quantification was performed using X200 magnified images of the 400-μm portion of the caudal part of the channels. Axons were counted manually and eight sections per animal were quantified. Progenitor cell differentiation inside the channels was quantified using the above-mentioned antibodies: Hu, NeuN, Olig2 and GFAP. Each slide was counter labeled with DAPI and GFP and cells were counted manually. Each cell type number was normalized to the total DAPI/GFP-labeled nuclei in the channels. Eight sections per animal were quantified. Quantification was performed using ImageJ.

Statistics and reproducibility

Two-group comparisons were tested by two-tailed Student's t-test (JMP software) at a designated significance level of $P < 0.05$. Multiple-group comparisons were tested by one-tail ANOVA (JMP software) at a designated significance level of $P < 0.05$, followed by post hoc analysis using Tukeys test. In vivo experiments were repeated three times, with similar results.

Electron microscopy

Detailed analysis of synapse formation and myelination of axons was performed using electron microscopy as follows: animals were perfused with 4% paraformaldehyde and 0.25% glutaraldehyde, and spinal cords were post-fixed with 1% osmium tetroxide, dehydrated and embedded in Durcupan resin. Semi-thin sections of 0.5 μm were stained with toluidine blue for general morphology. Sections (60 nm) were cut using an ultramicrotome and visualized using an FEI 200KV Sphera microscope at the UCSD CryoElectron Microscopy Core Facility.

Scanning electron microscopy imaging

Scanning electron microscopy (Zeiss Sigma 500) was used to image the patient-specific spinal cord scaffold. The scaffold was dehydrated in a series of ethanol baths and dried with a supercritical point dryer (Tousimis AutoSamdri 815A), and then sputter-coated with iridium using an Emitech K575X for 7 s at a deposition current of 85 mA. After sputter-coating, the scaffold was imaged using the Zeiss Sigma 500 scanning electron microscope at 5 kV.

Reporting Summary

Further information on research design is available in the Nature Research Reporting Summary linked to this article.

Data availability

Data supporting the findings of this study are available from ykoffler@ucsd.edu on reasonable request. All requests for materials and data are promptly reviewed by the Office of Innovation and Commercialization—University of California San Diego to verify whether the request is subject to any intellectual property or confidentiality obligations. Any materials and data that can be shared will be released via a Material Transfer Agreement.

Supplementary Material

Refer to Web version on PubMed Central for supplementary material.

Acknowledgements

References

1. Kadoya K, et al. Spinal cord reconstitution with homologous neural grafts enables robust corticospinal regeneration. Nat. Med 22, 479–487 (2016). [PubMed: 27019328]

2. Lu P et al. Long-distance growth and connectivity of neural stem cells after severe spinal cord injury. Cell 150, 1264–1273 (2012). [PubMed: 22980985]

3. NSCISC Annual Statistical Report - Model Systems Public Version (National Spinal Cord Injury Statistical Center, University of Alabama at Birmingham, 2014).

4. Murphy SV & Atala A 3D bioprinting of tissues and organs. Nat. Biotechnol 32, 773–785 (2014). [PubMed: 25093879]

5. Soman P, Chung PH, Zhang AP & Chen S Digital microfabrication of user-defined 3D microstructures in cell-laden hydrogels. Biotechnol. Bioeng 110, 3038–3047 (2013). [PubMed: 23686741]

6. Dalton PD, Flynn L & Shoichet MS Manufacture of poly(2-hydroxyethyl methacrylate-co-methyl methacrylate) hydrogel tubes for use as nerve guidance channels. Biomaterials 23, 3843–3851 (2002). [PubMed: 12164188]

7. Hung TK, Chang GL, Lin HS, Walter FR & Bunegin L Stress-strain relationship of the spinal cord of anesthetized cats. J. Biomech 14, 269–276 (1981). [PubMed: 7240289]

8. Tsai EC, Dalton PD, Shoichet MS & Tator CH Synthetic hydrogel guidance channels facilitate regeneration of adult rat brainstem motor axons after complete spinal cord transection. J. Neurotrauma 21, 789–804 (2004). [PubMed: 15253805]

9. Koffler J, Samara RF & Rosenzweig ES Using templated agarose scaffolds to promote axon regeneration through sites of spinal cord injury. Methods Mol. Biol 1162, 157–165 (2014). [PubMed: 24838966]

10. Gao M et al. Templated agarose scaffolds for the support of motor axon regeneration into sites of complete spinal cord transection. Biomaterials 34, 1529–1536 (2013). [PubMed: 23182350]

11. Gros T, Sakamoto JS, Blesch A, Havton LA & Tuszynski MH Regeneration of long-tract axons through sites of spinal cord injury using templated agarose scaffolds. Biomaterials 31, 6719–6729 (2010). [PubMed: 20619785]

12. Stokols S et al. Templated agarose scaffolds support linear axonal regeneration. Tiss. Eng 12, 2777–2787 (2006).

13. Stokols S & Tuszynski MH The fabrication and characterization of linearly oriented nerve guidance scaffolds for spinal cord injury. Biomaterials 25, 5839–5846 (2004). [PubMed: 15172496]

14. Stokols S & Tuszynski MH Freeze-dried agarose scaffolds with uniaxial channels stimulate and guide linear axonal growth following spinal cord injury. Biomaterials 27, 443–451 (2006). [PubMed: 16099032]

15. Lu P et al. Prolonged human neural stem cell maturation supports recovery in injured rodent CNS. J. Clin. Invest 127, 3287–3299 (2017). [PubMed: 28825600]

16. Lu P et al. Long-distance axonal growth from human induced pluripotent stem cells after spinal cord injury. Neuron 83, 789–796 (2014). [PubMed: 25123310]

17. Li J & Lepski G Cell transplantation for spinal cord injury: a systematic review. Biomed. Res. Int 2013, 786475 (2013). [PubMed: 23484157]

18. Park SS et al. Comparison of canine umbilical cord blood-derived mesenchymal stem cell transplantation times: involvement of astrogliosis, inflammation, intracellular actin cytoskeleton pathways, and neurotrophin-3. Cell Transplant. 20, 1867–1880 (2011). [PubMed: 21375803]

19. Peron S et al. A delay between motor cortex lesions and neuronal transplantation enhances graft integration and improves repair and recovery. J. Neurosc 37, 1820–1834 (2017).

20. Wang L et al. Early administration of tumor necrosis factor-alpha antagonist promotes survival of transplanted neural stem cells and axon myelination after spinal cord injury in rats. Brain Res. 1575, 87–100 (2014). [PubMed: 24887643]

21. Yu D et al. Blockade of peroxynitrite-induced neural stem cell death in the acutely injured spinal cord by drug-releasing polymer. Stem Cells 27, 1212–1222 (2009). [PubMed: 19418456]

22. Karimi-Abdolrezaee S, Eftekharpour E, Wang J, Morshead CM & Fehlings MG Delayed transplantation of adult neural precursor cells promotes remyelination and functional neurological recovery after spinal cord injury. J. Neurosci 26, 3377–3389 (2006). [PubMed: 16571744]

23. Zhu Y, Uezono N, Yasui T & Nakashima K Neural stem cell therapy aiming at better functional recovery after spinal cord injury. Dev. Dyn 247, 75–84 (2018). [PubMed: 28766845]

24. Fehlings MG, Sekhon LH & Tator C The role and timing of decompression in acute spinal cord injury: what do we know? What should we do? Spine 26, S101–S110 (2001). [PubMed: 11805616]

25. Tator CH, Fehlings MG, Thorpe K & Taylor W Current use and timing of spinal surgery for management of acute spinal surgery for management of acute spinal cord injury in North America: results of a retrospective multicenter study. J. Neurosurg 91, 12–18 (1999). [PubMed: 10419357]

26. Okada S The pathophysiological role of acute inflammation after spinal cord injury. Inflamm. Regen. 36, 20 (2016). [PubMed: 29259693]

27. Ciranna L Serotonin as a modulator of glutamate- and GABA-mediated neurotransmission: implications in physiological functions and in pathology. Curr. Neuropharmacol 4, 101–114 (2006). [PubMed: 18615128]

28. Harris KM & Weinberg RJ Ultrastructure of synapses in the mammalian brain. Cold Spring Harb. Perspect. Biol 4, a005587 (2012). [PubMed: 22357909]

29. Scannevin RH & Huganir RL Postsynaptic organization and regulation of excitatory synapses. Nat. Rev. Neurosci 1, 133–141 (2000). [PubMed: 11252776]

30. Armulik A et al. Pericytes regulate the blood-brain barrier. Nature 468, 557–561 (2010). [PubMed: 20944627]

31. Weiss N, Miller F, Cazaubon S & Couraud P O. The blood-brain barrier in brain homeostasis and neurological diseases. Biochim. Biophys. Acta 1788, 842–857 (2009). [PubMed: 19061857]

32. Basso DM, Beattie MS & Bresnahan JC Graded histological and locomotor outcomes after spinal cord contusion using the NYU weight-drop device versus transection. Exp. Neurol 139, 244–256 (1996). [PubMed: 8654527]

33. Iyer S, Maybhate A, Presacco A & All AH Multi-limb acquisition of motor evoked potentials and its application in spinal cord injury. J. Neurosci. Methods 193, 210–216 (2010). [PubMed: 20832429]

34. van Gorp S et al. Amelioration of motor/sensory dysfunction and spasticity in a rat model of acute lumbar spinal cord injury by human neural stem cell transplantation. Stem Cell Res. Ther 4, 57 (2013). [PubMed: 23710605]

35. Olson HE et al. Neural stem cell- and Schwann cell-loaded biodegradable polymer scaffolds support axonal regeneration in the transected spinal cord. Tissue. Eng. A 15, 1797–1805 (2009).

36. Pawar K et al. Biomaterial bridges enable regeneration and re-entry of corticospinal tract axons into the caudal spinal cord after SCI: Association with recovery of forelimb function. Biomaterials 65, 1–12 (2015). [PubMed: 26134079]

37. Wong DY et al. Macro-architectures in spinal cord scaffold implants influence regeneration. J. Neurotrauma 25, 1027–1037 (2008). [PubMed: 18721107]

38. Anderson MA et al. Astrocyte scar formation aids central nervous system axon regeneration. Nature 532, 195–200 (2016). [PubMed: 27027288]

39. Filous AR & Silver J Targeting astrocytes in CNS injury and disease: a translational research approach. Prog. Neurobiol. 144, 173–187 (2016). [PubMed: 27026202]

40. Fairbanks BD, Schwartz MP, Bowman CN & Anseth KS Photoinitiated polymerization of PEG-diacrylate with lithium phenyl-2,4,6-trimethylbenzoylphosphinate: polymerization rate and cytocompatibility. Biomaterials 30, 6702–6707 (2009). [PubMed: 19783300]

41. Yu CG, Joshi A & Geddes JW Intraspinal MDL28170 microinjection improves functional and pathological outcome following spinal cord injury. J. Neurotrauma 25, 833–840 (2008). [PubMed: 18627259]

42. Grill R, Murai K, Blesch A, Gage FH & Tuszynski MH Cellular delivery of neurotrophin-3 promotes corticospinal axonal growth and partial functional recovery after spinal cord injury. J. Neurosci 17, 5560–5572 (1997). [PubMed: 9204937]
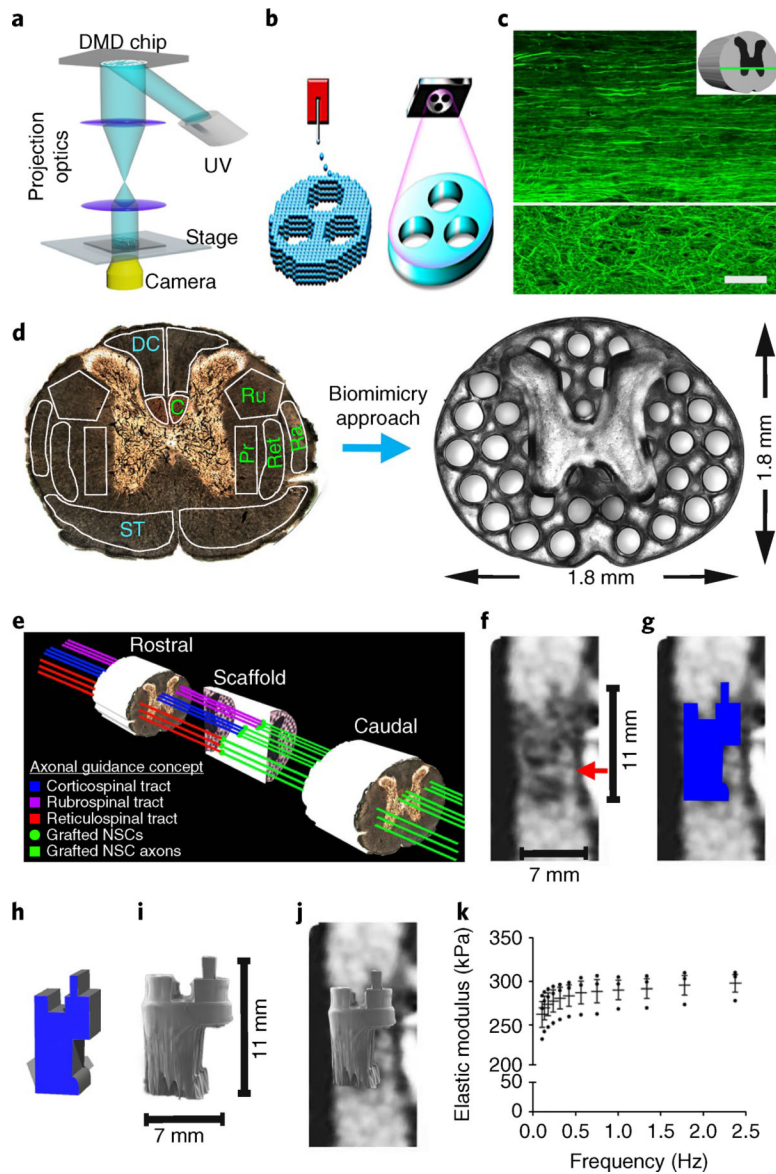
Fig. 1 |. The 3D-printed scaffold mimics the spinal cord architecture.
a, 3D-printer setup: an ultraviolet light source (365nm wavelength); a computer for sliced image-flow generation and system synchronization; a digital micromirror device (DMD) for optical pattern generation; a set of projection optics; a stage for sample position control; and a CCD (charge-coupled device) imaging system for on-line monitoring of the fabrication process. **b**, μCPP layerless 3D printing creates structures without discrete layers. In extrusion-based 3D-printing approaches (left), as the stage moves in the z axis and material is extruded, layers are created between the drops. μCPP printing (right) creates a structure with one continuous layer. **c**, Heavy chain neurofilament (NF200) labeling of axons in intact T3 rat spinal cord. Rostral is to the left, and caudal is to the right of the image. The axons in the white matter (top of the panel) are highly organized into parallel arrays traveling from rostral to caudal. The axons in the gray matter (bottom of the panel) are not linear. The white line demarcates the interface between the white and gray matter. The inset schematic

diagram indicates the orientation of the horizontal section. **d**, Axonal projections in the spinal cord are linearly organized into regions (fascicles) containing axons of related function. Motor systems are shown in green and sensory systems are shown in blue. C, corticospinal tract; Ru, rubrospinal tract; Ra, raphespinal tract; Ret, reticulospinal tract; Pr, propriospinal tract; ST, dpinothalamic tract; DC, dorsal column sensory axons. Our scaffold mimic the linear organization of white matter. Channels are precisely printed in 3D space. **e**, A schematic diagram explaining the axonal alignment and guidance hypothesis. A lesioned host axon (for example, a corticospinal tract (CST), rubrospinal or reticulospinal axon) regenerates into the scaffold and forms a synapse onto a NPC-derived axon inside a channel, and the NPC neuron in turn extends an axon out of the scaffold below the injury site (green lines) into the same white matter fasciculus below the lesion, guided by a linear microchannel. The scaffold maintains its 3D coordinates across the lesion, matching the natural host architecture. **f**, A sagittal mid-cervical T1-weighted magnetic resonance image of a human clinically complete (ASIA A) SCI. A sliver of spared host white matter is evident on the anterior aspect (right side) of the lesion (arrow). The size of the lesion is noted next to the image. **g**, The traced outline of the cystic lesion cavity from **f**. **h**, A computer-aided design (CAD) 3D model of the scaffold to be 3D-printed, corresponding to the precise lesion shape. **i**, The printed scaffold matches the size shown in **f**. **j**, A hypothetical fit of the printed 3D scaffold in a human contusion cavity. **k**, Mechanical measurement of the scaffold elastic modulus using dynamic mechanical analysis. $n = 3$ scaffold samples tested by dynamic mechanical analysis. The data are presented are means± s.e.m. Scale bar, 50μm (**c**).
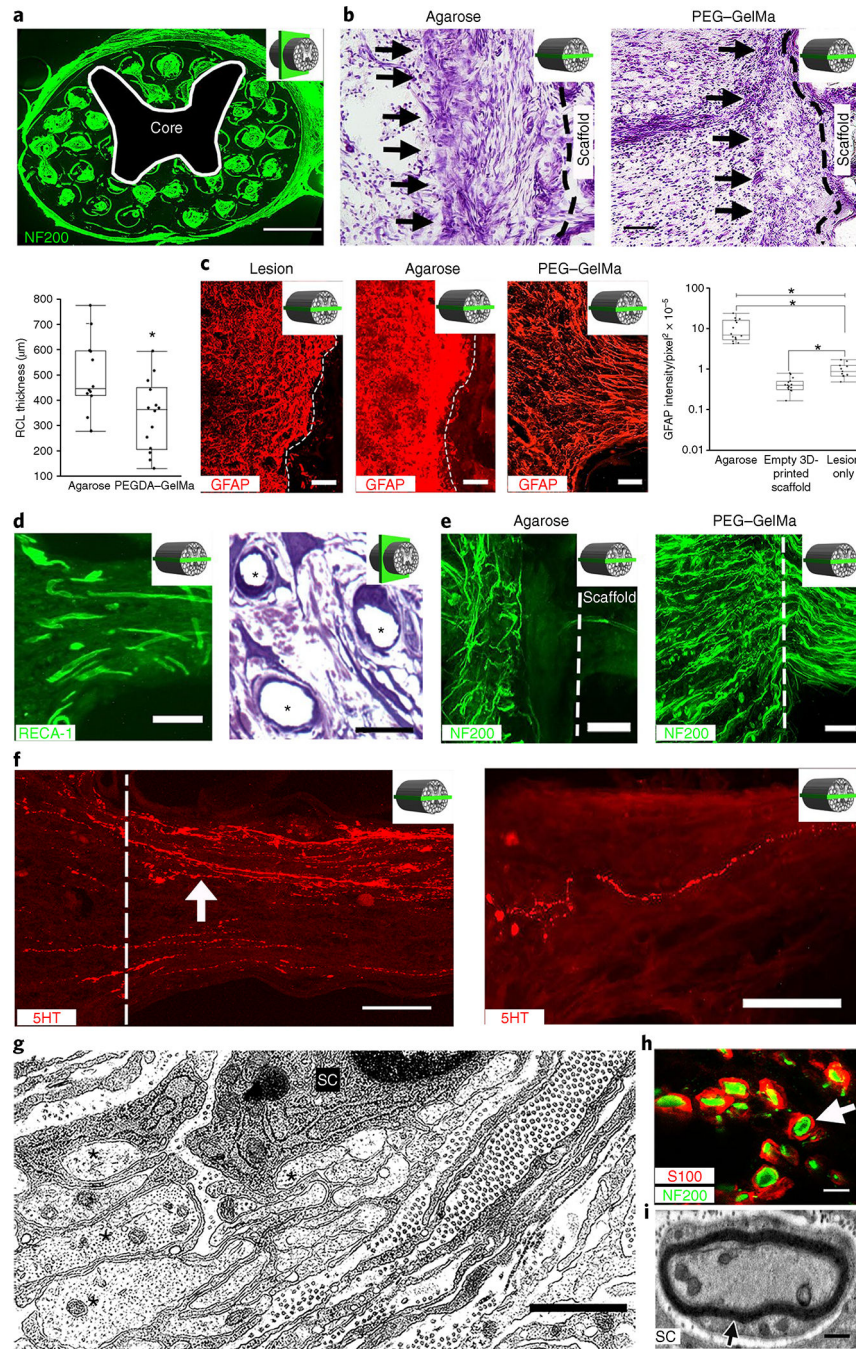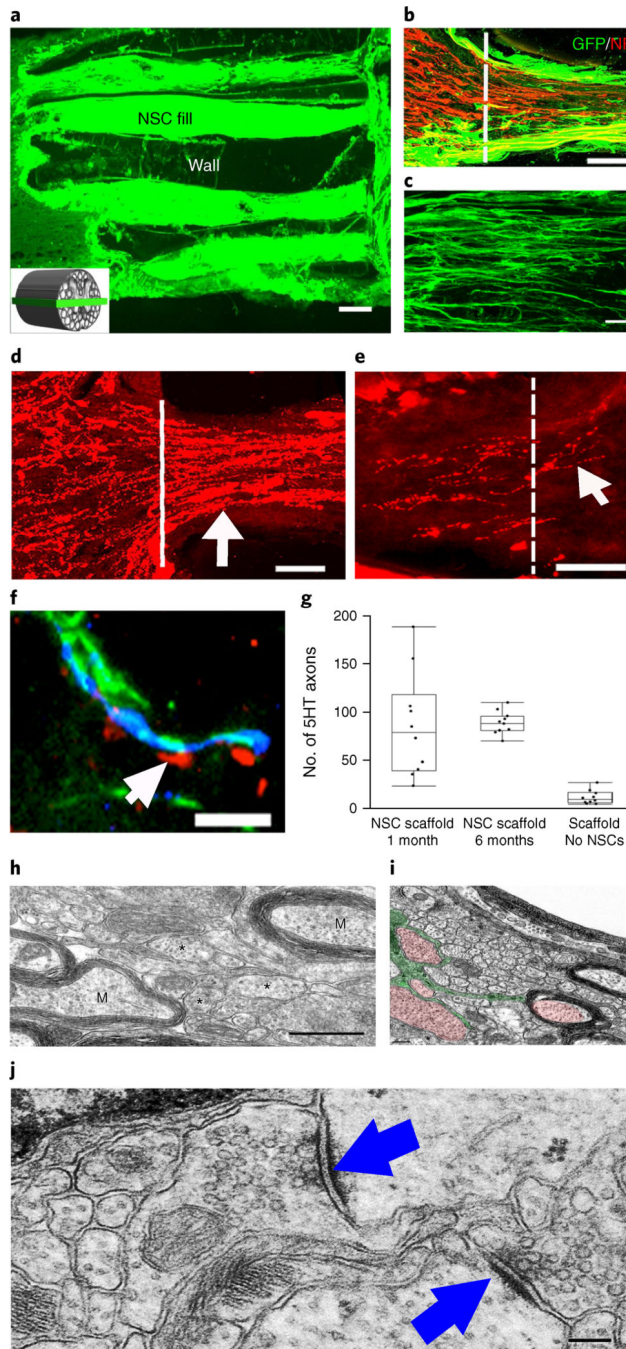
Fig. 2 |. Four weeks in vivo performance of empty 3D-printed scaffold implants.
a, A cross-section through an implanted scaffold labeled for axons (NF200). The inset
schematic diagrams indicate the section orientation. **b**, Nissl stain reveals a reactive cell
layer (arrows) at the site of implantation of an agarose scaffold (left) or a PEGDA-GelMa
scaffold (right). Rostral is to the left and caudal is to the right. The black dashed line
demarcates the interface of the host spinal cord with the scaffold. The box and whisker plot
shows the quantification of the mean reactive cell layer (RCL) thickness. The boxes show
the 25th-75th percentile range, and the center line is the median. Whiskers show 1.5 times

the interquartile range (IQR) from the 25th or 75th percentile values. *$P < 0.0019$ (Student's *t*-test), $n = 12$ animals. **c**, A host glial 'scar' is revealed by GFAP immunoreactivity in animals with lesion only (no scaffold) (left), an agarose scaffold (middle) or a 3D-printed scaffold (right). Rostral is to the left and caudal is to the right. In the 3D-printed scaffold, the glial processes align longitudinally with the channels. The box and whisker plot shows the quantification of the mean GFAP intensity in the host spinal cord surrounding the lesion site. The boxes show the 25th-75th percentile range, and the center mark is the median. Whiskers show 1.5 times IQR from the 25th or 75th percentile values. *$P < 0.0001$ (one-tailed ANOVA with post hoc Tukey's), $n = 11$ animals. **d**, Scaffold vascularization shown by RECA-1 immunolabeling (left) and toluidine blue stain (asterisks indicate vessels) (right). **e**, Left, Host axons (labeled for NF200) do not enter agarose scaffolds. Right, Host axons enter 3D-printed scaffolds. The dashed line indicates the host/scaffold interface on the rostral end of the lesion site. **f**, Host 5HT-labeled serotonergic axons (white arrow) regenerate into an empty scaffold (left) and reach the caudal end of the channel (right). The white dashed line demarcates the rostral entrance to the channel. **g**, Electron microscopy within a channel demonstrates axons (asterisks) associated with a neighboring ensheathing Schwann cell (SC). **h**, A magnified view of a channel in **a** showing S100-labeled Schwann cells ensheathing NF200-labeled axons (arrow). **i**, Electron microscopy of a channel demonstrates a myelinated axon in the scaffold with a Schwann cell. Scale bars, 500 μm (**a**), 200 μm (**b**), 100 μm (**c**,**e**), 25 μm (**d**, left), 20 μm (**d**, right), 50 μm (**f**), 1 μm (**g**), 5 μm (**h**), 0.5 μm (**i**).
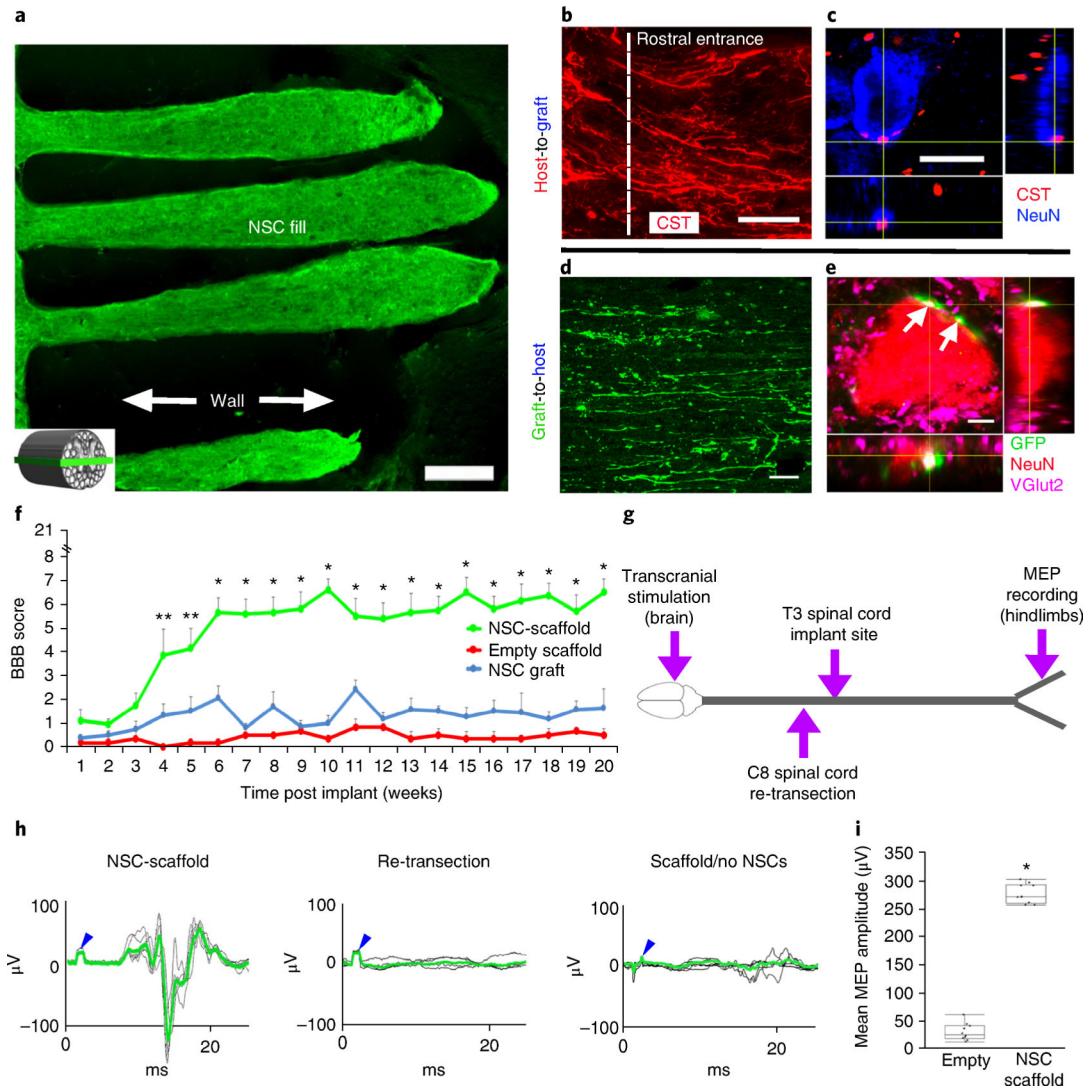
Fig. 3 |. Four weeks in vivo performance of NPC-loaded 3D-printed scaffold implants.
a, Channels are filled with GFP-expressIng NPCs. The inset schematic diagram indicates the orientation of the horizontal sections in all panels of this figure. **b**, The rostral entrance to the channel is penetrated by host axons (labeled for NF200 (NF)); the host axons are distinguished from graft-derived axons by the absence of GFP expression. **c**, Implanted GFP-expressing NSCs extend linear axons within the scaffold. Rostral is to the left and caudal is to the right. **d**, 5HT-labeled host serotonergic axons enter the NPC-filled channel from the rostral (left) aspect of the lesion and regenerate linearly in the channel (arrow). **e**,

5HT-labeled host axons exit the caudal aspect of the channel to regenerate into the host spinal cord distal to the lesion (arrow). The white line demarcates the exit from the caudal channel to the caudal spinal cord. **f**, 5HT host axons regenerating into scaffold channels form appositional contacts (arrows) with dendrites (MAP2) of implanted NPCs (labeled for GFP). **g**, Quantification of the mean number of 5HT axons reaching the caudal end of the scaffold (one-tail ANOVA $P < 0.0322$, post hoc Tukey's), $n = 10$ animals. The boxes show the 25th-75th percentile range, and the center mark is the median. Whiskers show 1.5 times IQR from the 25th or 75th percentile values. **h**, At the ultrastructural level, axons of varying diameters (asterisks) are present within channels and many axons are myelinated (M). **i**, An ultrastructural image showing an oligodendrocyte (green) sending multiple processes to myelinate and ensheath axons (red). **j**, Synapses (arrows) form between axons within channels and the dendrites of implanted NPCs. The synapses are asymmetric with presynaptic boutons containing rounded vesicles. Scale bars, 200 μm (**a**), 50 μm (**b**), 10 μm (**c**,**f**), 100 μm (**d**,**e**), 500 nm (**h**), 0.2 μm (**i**), 200 nm (**j**).

Fig. 4 |. Long-term in vivo studies of 3D-printed scaffolds loaded with NPCs.
a-e, Anatomy at 6 months post implant. **a**, The channels are structurally intact and filled with GFP-expressing NPCs. The inset schematic diagram indicates the orientation of the horizontal sections in all panels of this figure, with rostral to the left. **b**, Corticospinal axons enter the scaffold and extend linearly in a caudal direction. **c**, CST axons converge on a NeuN-labeled neuron inside the channel, forming bouton-like contacts with the soma. **d**, GFP axons extend out from the scaffold into the host white and gray matter caudal to the lesion. Ventrolateral white matter, 2 mm caudal to the lesion. **e**, NPC-derived GFP-labeled axons form excitatory contacts (VGlut2) on gray matter host neurons (labeled for NeuN) located 2 mm caudal to the lesion (white arrows). **f-i**, Behavioral studies. **f**, BBB motor scores after complete transection (repeated-measures ANOVA; **$P < 0.0232$, *$P < 0.0008$; mean±s.e.m, $n = 10$ animals). **g**, Schematic diagram of the electrophysiology study performed at 6 months post implant. Transcranial electrical stimulation is applied to the motor cortex in the brain and MEPs are recorded from the hindlimbs. **h**, Rats with 3D-printed, NPC-filled scaffolds exhibit MEP responses that are abolished by subsequent re-

transection of the spinal cord immediately above the scaffold. Animals with empty scaffolds show no MEPs. The blue arrowheads mark stimulation artifacts. The green lines represent averages of several individual stimulations shown in black. **i,** The mean MEP amplitude is significantly greater in animals implanted with NPC-containing scaffolds. The boxes show the 25th-75th percentile range, and the center mark is the median. Whiskers show 1.5 times IQR from the 25th or 75th percentile values. (Student's *t*-test; *P* < 0.0001, n = 10 animals). Scale bars, 250μm (**a**), 50μm (**b**), 10μm (**c**), 40μm (**d**), 5μm (**e**).